KSCE Journal of Civil Engineering (2024) 28(5):1657-1674
DOI 10.1007/s12205-024-2479-0

pISSN 1226-7988, eISSN 1976-3808
www.springer.com/12205

Geotechnical Engineering

Seismic Bearing Capacity of Strip Footings with Modified Pseudo-dynamic Method

Xudong Kang[a], **Jianqun Zhu**[b], **and Lili Liu**[a]

[a]*School of Civil Engineering, Central South University, Hunan 410075, China*
[b]*Changzhou Institute of Technology, Department of Civil & Architecture Engineering, Changzhou 213032, Jiangsu, China*

ARTICLE HISTORY

Received 4 January 2023
Revised 18 September 2023
Accepted 6 December 2023
Published Online 15 February 2024

KEYWORDS

Nonlinear criterion
Piece-wise
Bearing capacity
Modified pseudo-dynamic method

ABSTRACT

Current research has shown a nonlinear trend in the failure of soil, and the single tangent method is commonly adopted when coping with nonlinear problems of soil failure. However, the method equates a nonlinear criterion to an optimizable linear criterion, which may differ from the actual situation, resulting in conservative results. In this paper, two types of piece-wise log-spiral failure mechanisms for bearing capacity estimations, including symmetrical and unilateral mechanisms were proposed with the nonlinear Mohr-Coulomb criterion. The static bearing capacity of foundations was evaluated using the symmetric failure mechanism, while the seismic bearing capacity of foundations was evaluated adopting a modified pseudo-dynamic method based on the unilateral failure mechanism. The result shows that the bearing capacity calculated in the paper is smaller compared to the result using the linear Mohr-Coulomb criterion. For London clay, the static bearing capacity is reduced by about 45% at a foundation width equal to 1m. From the comparisons, it is found that the proposed approach of piece-wise log-spiral failure mechanism for bearing capacity estimation is effective. In addition, parametric studies show that the nonlinear parameters, the initial factor of seismic acceleration, the normalized frequency, and the damping ratio all have obvious effects on the seismic bearing capacity. A significant reduction in the seismic bearing capacity of the foundation occurs when the normalized frequency $\omega_s H/V_s$ is equal to $(0.5 + n)\pi$ $(n = 0, 1, 2, \cdots)$. Considering that the approach proposed provides a strict upper bound to the bearing capacity, the result imparts confidence in the approach of analysis presented.

1. Introduction

The bearing capacity assessment approaches for foundations can be broadly divided into the four categories as follows: (a) the limit analysis approach, (b) the limit equilibrium approach, (c) stress characteristics approach, and (d) numerical analysis. Among the above approaches, the limit equilibrium approach is extensively used due to its simplicity of formulation. However, regardless of the analysis approach used, previous studies generally followed the linear Mohr-Coulomb (MC) criterion. Although the research on nonlinear criterion has been developed, the essence of most approaches is to linearize it, so the study on how to truly characterize the nonlinearity of geotechnical material failure is essential.

Prandtl adopted the ideal rigid plastic theory with linear MC criterion, the shape of the sliding surface of rigid strip foundation pressed into c and φ soil and the corresponding formula of ultimate bearing capacity is obtained. Based on Prandtl sliding surface, the effect of uniformly distributed load q was added, and the bearing capacity of weightless and cohesionless materials was obtained. Considered the influence of the soil weight, Terzaghi (1943) divided the failure mechanism into three parts, contain two rigid triangles and the shear zone, in which the shear zone was consist of a logarithmic spiral curve equation, its conclusion formula is presented as follow:

$$p_u = 0.5\gamma B N_\gamma + cN_c + qN_q\,. \tag{1}$$

In addition, Soubra (1999) calculated the foundation bearing

CORRESPONDENCE Jianqun Zhu ✉ zhu-jq@163.com Changzhou Institute of Technology, Department of Civil & Architecture Engineering, Changzhou 213032, Jiangsu, China

capacity following a multi-block failure mechanism. After that, many scholars contributed to related research. Most of the above studies used the linear MC criterion, but extensive experimental investigations have indicated that linear damage is only a special case, and geotechnical media tend to obey nonlinear damage.

Zhang and Chen (1987) introduced the nonlinear failure criterion, the development of bearing capacity of foundation and slope stability research following the nonlinear failure criterion has increased step by step. Drescher and Christopoulos (1988) first combined the nonlinear yielding conditions with limit analysis, and constructive suggestions for subsequent research are presented. Hoek (1990) linearized the Hoek-Brown criterion using the single tangent approach and estimates the bearing capacities based on the failure criterion after linearization. Its shear strength parameters were related to the location of the tangent point on the strength envelope. The normal stress in the solution area was assumed to be the same, which was inconsistent with the engineering practice. Yang and Yin (2005) employed the generalized tangential technique and combined it with upper bound analysis to solve the problems of slope stability. The essence of the approach was to linearize the nonlinear failure criterion and to analyze the foundation bearing capacity. Fraldi and Guarracino (2009) adopted the variational approach to deal with the Hoek-Brown criterion and studied the tunnel collapse problem. Serrano et al. (2016) combined the characteristic approach and the power-law criterion to study the bearing capacity of strip foundation on the weightless soil. Yu et al. (2019) considered the nonlinear MC criterion and pore pressure, employed three-dimensional failure mechanisms to assess tunnel collapse issues. AlKhafaji et al. (2020) estimated the problem of bearing capacity of rock foundations employing the modified Hoek-Brown criterion, and the effect of horizontal seepage force was considered. However, the mechanisms used were still the traditional multi-wedge failure mechanisms. Ganesh and Kumar (2021) assessed the bearing capacity of both rough and smooth foundations employing the stress characteristic approach based on the nonlinear failure criterion. However, fewer specifically researches have been executed so far to calculate the foundation bearing capacity following upper bound analysis considering a nonlinear MC criterion. And most of the studies only linearized the nonlinear criterion, the results were conservative (Yang and Huang, 2011). Michalowski and Park (2020) put forward a collapse mechanism for slope stability analysis with the Hoek-Brown criterion, and obtained a more optimal solution. The collapse mechanism was divided into n blocks, each with its own unique rupture angle, thus corresponding to the variation of the strength envelope. The above study provided the idea for performing the analysis without affecting real nonlinear pressure dependency of the strength criterion.

For the assessment of seismic bearing capacity of foundations, initially most scholars used the pseudo-static method (Dormieux and Pecker, 1995; Kumar and Mohan Rao, 2002; Cascone and Casablanca, 2016; Pane et al., 2016; Conti, 2018; Zhang et al., 2021; Beygi et al., 2022), but the seismic action is a dynamic corresponding process, so some scholars adopted the pseudo-dynamic method afterwards (Ghosh, 2008; Zhong et al., 2022; Chen et al., 2022). However, the pseudo-dynamic approach did not consider the zero-stress boundary condition of the free surface and the effect of the damping ratio of the soil. Therefore, Bellezza (2014) proposed a modified pseudo-dynamic method. Subsequently, some scholars adopted this method for their studies (Soufi et al., 2021; Tavakoli et al., 2022).

Ganesh and Kumar (2022) evaluated the seismic bearing capacity of rough strip foundations using the stress characterization method based on the nonlinear MC criterion, however, the dynamic characteristics of seismic forces were not considered. Nadgouda and Choudhury (2021) investigated the seismic bearing capacity coefficient of foundations on dry sand using the modified pseudo-dynamic method. Xu and Zhou (2023) studied the seismic bearing capacity of foundations on unsaturated soils using the modified pseudo-dynamic method. But the two studies above did not consider the nonlinear damage characteristics of the soil. Liu et al. (2022) investigated the seismic bearing capacity of rock foundations using the modified pseudo-dynamic method, but it does not truly reflect the characteristics of nonlinear damage of geotechnical bodies because it still uses the single tangent method to deal with the Hoek-Brown criterion.

Therefore, following the upper bound method, this paper proposed two types of piece-wise log-spiral failure mechanisms for bearing capacity estimations considering the nonlinear failure criterion of geotechnical materials. Changing the traditional way of thinking about analysis and establishing two modified failure mechanisms. The case of no seismic is considered using a symmetrical failure mechanism, and the case of seismic is considered based on a unilateral failure mechanism and the modified pseudo-dynamic approach. The optimal solution of the static and seismic bearing capacity can be obtained employing the genetic algorithm (GA), and the approximate stress distribution of part of the fracture surface is depicted. To confirm the feasibility of the used approach, the results are compared with results from previous literature, and the influence of the nonlinear parameters is discussed. In addition, the influence of the MPD parameters on seismic bearing capacity is analyzed according to the unilateral failure mechanism. The analysis shows that a better upper limit solution can be obtained using the approach proposed in the paper. The approach provides a new idea for the seismic bearing capacity calculation of foundations resting on c and φ soil.

2. Methodology

2.1 Nonlinear Mohr-Coulomb Criterion

The maximum principal stress σ_1 and the minimum principal stress σ_3 are linearly related in the MC criterion, as shown in Fig. 1. The formula is as follows.

$$\sigma_1 = q_p + M_p \sigma_3 , \tag{2}$$

with the material parameters defined as

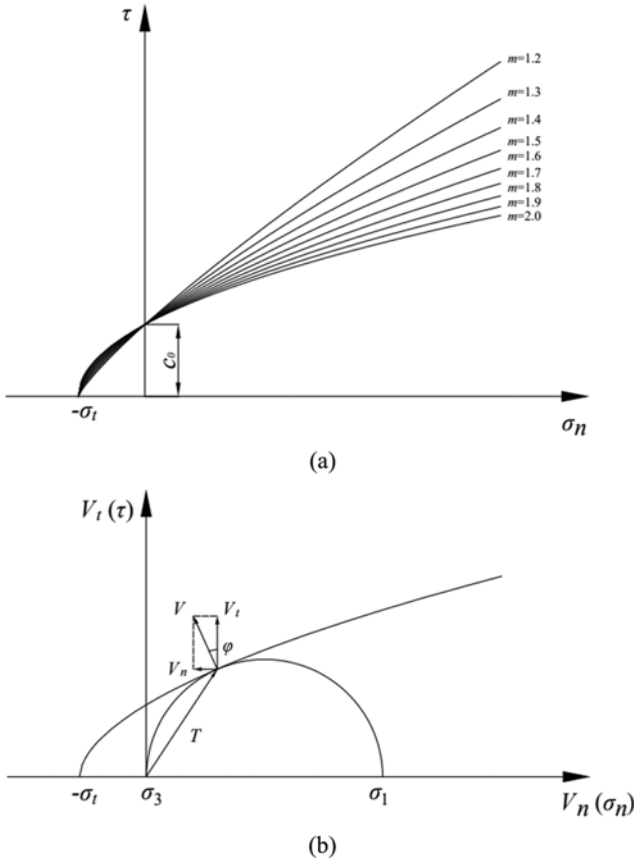

Fig. 1. Nonlinear Mohr-Coulomb Failure Envelope: (a) Shear Stress and Normal Stress, (b) Stress Vector *T*

$$q_p = \frac{2c\cos\varphi}{(1-\sin\varphi)}, \tag{3}$$

$$M_p = \frac{(1+\sin\varphi)}{(1-\sin\varphi)}, \tag{4}$$

where q_p and M_p are the shear strength index of soil. However, many experiments have shown that the damage of soil follows a nonlinear criterion. To make the calculation convenient, the nonlinear strength criterion of soil is generally expressed by normal stress and tangential stress. A variety of expressions have been proposed in the previous literature, but the proposed formulas are in power exponential form, and the parameters can be converted to each other. The expression adopted in this paper is as follows:

$$\tau = c_0\left(1+\frac{\sigma_n}{\sigma_t}\right)^{1/m} \tag{5}$$

where c_0 is the cohesion at zero normal stress, and τ, σ_n, σ_t and m are the shear stress, the normal stress, the tensile stress, and the nonlinear parameter, respectively. When the value of m is 1, the nonlinear criterion parameter can be equivalent to the linear MC criterion parameter. Generally, the failure characteristics of soil under different stress conditions are obtained through the triaxial test, and then the parameters of the nonlinear MC criterion are calculated in the fitting approach.

2.2 Piece-Wise Method

Two main methods combine the limit analysis theorem with the nonlinear criterion: variational principles and generalized tangential technique. Generalized tangential technique is widely adopted due to its convenience, which proposed by Yang and Yin (2004). The principle of the above method is to replace the nonlinear strength envelope with the tangent of a point on the failure envelope. Therefore, the strength of other points on the tangent must be larger than the true shear strength of materials. According to the theory, the upper limit solution of the tangent is the upper bound of the real ultimate load, which is widely used.

In this paper, the piece-wise log-spiral method is adopted. It is necessary for the subsequent study of the paper that the nonlinear criterion can be written as a connection between shear stress τ and normal stress σ_n. Then, transforms Eq. (5) into a parametric equation about the angle φ in Eqs. (6) and (7). The meaning of the angle φ will be explained in the following sections.

$$\sigma_n = \sigma_t\left(\frac{m\sigma_t\tan\varphi}{c_0}\right)^{m/(1-m)} - \sigma_t \tag{6}$$

$$\tau = c_0\left(\frac{m\sigma_t\tan\varphi}{c_0}\right)^{1/(1-m)} \tag{7}$$

The piece-wise log-spiral method cannot be discussed in isolation and is a treatment that closely links the nonlinear failure criterion to a specific failure mechanism. The method is reflected in the fact that it uses multiple points on the failure envelope, and it's essentially a modified application of the multiple tangent method. The details of the presentation are discussed in the following sections.

2.3 Modified Pseudo-Dynamic Method

Compared with the traditional pseudo-dynamic method, the method takes into account the zero stress boundary condition of the free surface and the influence of the damping ratio of the geotechnical body (Bellezza, 2014), and its main equation is as follows:

$$a_h(z,t) = \frac{a_{h0}}{(C_s^2+S_s^2)}[(C_sC_{sz}+S_sS_{sz})\cos(\omega_s t)+(S_sC_{sz}-C_sS_{sz})\sin(\omega_s t)], \tag{8}$$

$$k_h(z,t) = \frac{k_h}{(C_s^2+S_s^2)}[(C_sC_{sz}+S_sS_{sz})\cos(\omega_s t)+(S_sC_{sz}-C_sS_{sz})\sin(\omega_s t)], \tag{9}$$

$$a_{h0} = k_h g, \tag{10}$$

$$C_{sz} = \cos\left(\frac{y_1 z}{H}\right)\cosh\left(\frac{y_2 z}{H}\right), \tag{11}$$

$$S_{sz} = -\sin\left(\frac{y_1 z}{H}\right)\sinh\left(\frac{y_2 z}{H}\right), \tag{12}$$

$$C_s = \cos(y_1)\cosh(y_2), \tag{13}$$

$$S_s = -\sin(y_1)\sinh(y_2), \tag{14}$$

$$y_1 = \frac{\omega_s H}{V_s}\sqrt{\frac{\sqrt{1+4\xi^2}+1}{2(1+4\xi^2)}}, \tag{15}$$

$$y_2 = -\frac{\omega H}{V_s}\sqrt{\frac{\sqrt{1+4\xi^2}-1}{2(1+4\xi^2)}}, \tag{16}$$

where ω_s is the angular frequency, ξ is the damping ratio, k_h is the initial factor of seismic acceleration, H is the depth to bedrock, y_1 and y_2 are constants, and g is the acceleration of gravity, V_s is the velocity of the shear wave.

3. Seismic and Static Bearing Capacity

3.1 Failure Mechanism of Foundation

Various foundation failure mechanisms are proposed by many scholars. Thus, the selection of the failure mechanism leading to the reduction of the maximum dissipated energy rate is the key point for analyzing the foundation bearing capacity. Combined with the nonlinear MC criterion, two types of piece-wise log-spiral failure mechanisms for strip footing, including symmetrical and unilateral mechanisms were established in this paper. The failure mechanism in which bilateral symmetry is selected as an example is described as follows. The soil body under the strip foundation is divided into three parts (right side half). Each part moves or rotates as a whole. As the mechanism is symmetrical, the right half of the mechanism is presented in Fig. 2, which is consist of rigid body ABC, log-spiral plastic zone BCD, and rigid body BDE. Only the rigid body ABC is beneath the foundation in the failure mechanism. Energy dissipation occurs in the velocity discontinuity surface and inside the plastic zone. It should be emphasized that it is assumed that DE in the mechanism is tangent to the curve CD, so there is no energy dissipation on BD. The first block of the plastic zone BCD's velocity hodograph is presented in Fig. 3 and v_{CB} is obtained.

Different from other failure mechanisms, the log-spiral plastic zone BCD is mainly explained, as shown in Fig. 4. When the foundation is damaged, the plastic zone rotates around point B. A rupture surface is depicted by line $C_0C_jC_n$, which can be thought of as a thin zone of the soil that comes under a significant velocity gradient over its thickness. It is noted that the rupture surface is made up of multiple logarithmic spirals and is piece-wise. Along the rupture surface $C_0C_jC_n$, its stress reaches the limit state described by the nonlinear MC criterion in Eq. (5), and components of stress vector T also reach the limit of rupture, as presented in Fig. 1(b). As expected by the normality flow rule, the properties of geotechnical materials are dominated by pressure, and volumetric strain impacts the shearing stress along surface $C_0C_jC_n$. To accommodate this strain in the failure mechanism, the velocity discontinuity vector is inclined to the rupture surface $C_0C_jC_n$ at rupture angle φ. Therefore, the logarithmic spiral is chosen as the shape of the rupture surface. The rupture angle φ changes along with the failure criterion (Fig. 1(b)), the plastic zone BCD in Fig. 4 is separated into n sectors, each sector with a separate, and the uncertain constant value of the rupture angle φ. Although the BCD region revolves as a whole, each sector's rupture surface is regulated by a separate rupture angle φ. The BCD region is divided into several parts, which are perfectly combined with the strength envelope, the non-linearity of the strength envelope and non-uniformity of the rupture surface are considered. The failure surface $C_0C_jC_n$ is unsmooth but continuous at points C_j. This ensures that the BCD region rotates around point B.

The width of the jth sector of the plastic zone BCD is restricted by its vertex angle η_j, and the radial length of sector j are restricted by the angle θ_{j-1} and θ_j (Fig. 4). As shown in Fig. 1, with the change of the rupture angle φ, the stress vector T acting on the failure surface $C_0C_jC_n$ changes accordingly. However, such a stress vector T does not exist in equilibrium state of a stress field, but the upper bound approach does not require equilibrium.

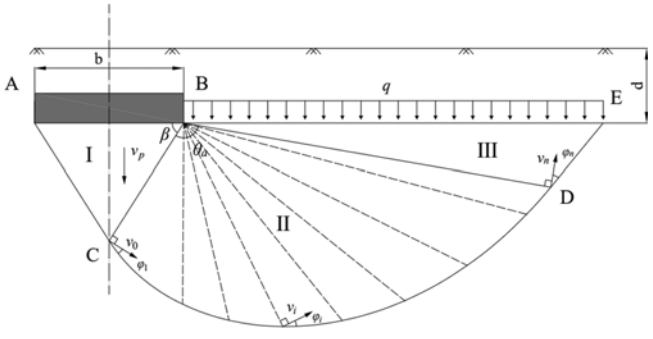

Fig. 2. Bilateral Failure Mechanism of Foundation (the Right Part)

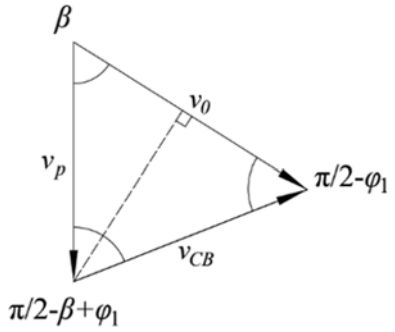

Fig. 3. Velocity Hodograph for the First Block of the BCD

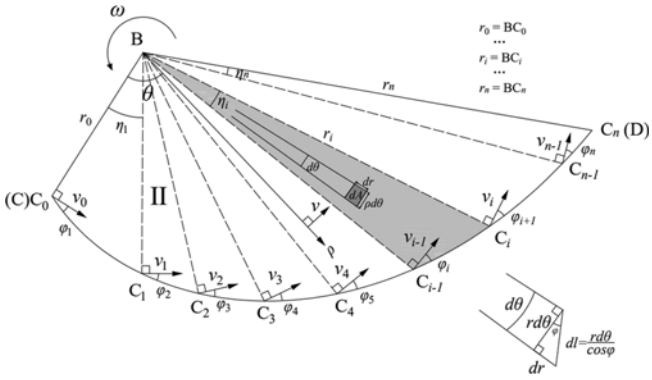

Fig. 4. Detailed Failure Mechanism of the BCD

The failure mechanism can essentially be seen as a modification of the traditional Prandtl failure mechanism, and the above mechanism can better match the nonlinear failure criterion compared with the traditional Prandtl failure mechanism and the multi-wedge discretization system. To make the approach simpler and more universal, the following assumptions are made. The strip foundation is long enough, and the issue can be considered as a plane strain issue. The soil conforms to the associated flow rule. The damage of the soil body is restricted by the nonlinear MC criterion, as shown in Eq. (5). The failure angle of rigid body ABC and rigid body BDE is the same as that of the sector in their respective adjacent BCD. The line AC is tangent to the curve C_0C_1, and the line DE is tangent to the curve $C_{n-1}C_n$.

Polar radius r of each sector is decided by the following logarithmic spiral formula

$$r = r_{j-1}e^{(\theta-\theta_{j-1})\tan\varphi_j},\ \theta_{j-1} \le \theta \le \theta_j . \tag{17}$$

Radii r_j (j = 1, 2, 3, 4 … n) are the line BC_j (Fig. 4), and are decided by the formula below

$$r_j = r_0\prod_{k=1}^{j} e^{\eta_k\tan\varphi_k} = r_0 e^{\sum_{k=1}^{j}\eta_k\tan\varphi_k}, \tag{18}$$

$$r_0 = \frac{b}{2\cos\beta}, \tag{19}$$

where $\eta_j = \theta_j - \theta_{j-1}$.

Above is a detailed description of the symmetric failure mechanism, a unilateral failure mechanism considering the effect of seismic forces is established as shown in Fig. 5.

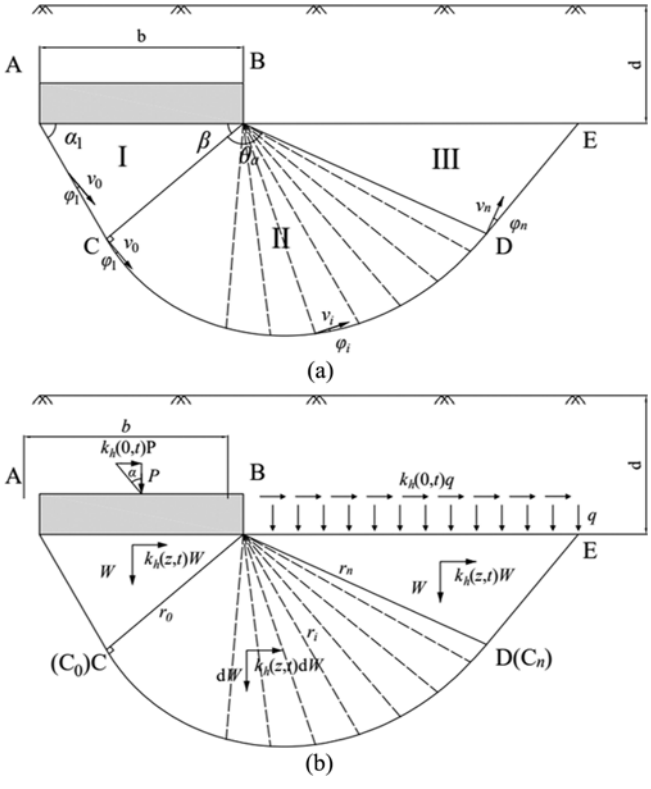

Fig. 5. Unilateral Failure Mechanism of Foundation: (a) Speed Chart, (b) Force Diagram

3.2 Formation of Work-Balance Equation

According to the theorem of virtual work, for a rigid plastic object with volume V and surface area S, the virtual internal power of static allowable stress field σ_{ij} on virtual strain rate $\dot{\varepsilon}_{ij}$ is equal to the virtual external work power of external force F_i and p_i on any motion allowable velocity field v_i^*, and the expression is as follows.

$$\int_V F_i v_i^* dV + \int_S p_i v_i^* dS = \int_V \sigma_{ij}\dot{\varepsilon}_{ij}^* dV \tag{20}$$

Consequently, the upper bound method can be deduced: among all the limit loads corresponding to any allowable velocity field, the real limit load is the smallest. In other words, for any kinematically admissible velocity field, the rate at which actual forces perform work is tantamount to the rate at which energy is dissipated. The upper bound approach of limit analysis so far is widely employed to evaluate engineering geological problems (Yang et al., 2004; Fraldi and Guarracino, 2009; Yang and Wang, 2011; Huang and Liu, 2016; Li et al., 2021; Zhong and Liao, 2022). Therefore, this study employs limit analysis, as shown in the following formula:

$$\dot{D}_{\text{int}} = \dot{W}_{\text{ext}}, \tag{21}$$

where $\dot{D}_{\text{int}}$ means the power of the internal force, and $\dot{W}_{\text{ext}}$ means the power of the external force.

3.2.1 Symmetrical Failure Mechanism

External force power includes vertical central load P on the foundations, uniformly distributed load q, and soil weight. According to the hypothesis proposed in this paper, the internal force power includes four parts: the velocity discontinuity BC, the fracture surface $C_0C_jC_n$, the plastic zone BCD, and the fracture surface DE. The power of the vertical central load P can be expressed as follows:

$$v_p = v_0\frac{\cos\varphi_1}{\cos(\beta-\varphi_1)}, \tag{22}$$

$$\dot{W}_1 = \frac{1}{2}\omega r_0 P\frac{\cos\varphi_1}{\cos(\beta-\varphi_1)}, \tag{23}$$

where v_0 is the velocity magnitude of the rupture surface of the first part of the plastic zone BCD, β is an internal angle of the rigid body ABC (Fig. 2), and φ_1 is the failure angle of Part 1 in BCD of the plastic zone. The power of the uniformly distributed load q can be expressed as follows:

$$\dot{W}_2 = -\omega q\cdot\overline{BE}\cdot r_n\cos(\pi-\beta-\theta_a), \tag{24}$$

$$\overline{BE} = \frac{r_n\cos\varphi_n}{\cos(\pi-\beta-\theta_a+\varphi_n)}, \tag{25}$$

where v_n is the value of the velocity on the line DE, θ_a is the vertex angle of the plastic zone BCD (Fig. 2), and φ_n is the

failure angle of Part n in BCD of the plastic zone. The rate of the rigid body ABC weight takes the form

$$\dot{W}_3 = \frac{1}{8}\omega\gamma b^2 \tan\beta r_0 \frac{\cos\varphi_1}{\cos(\beta-\varphi_1)}, \tag{26}$$

where γ is the unit soil weight, and b is strip footing width. Integrating the area of the plastic zone BCD, the infinitesimal micro-element dA is depicted in Fig. 4, and the plastic zone BCD gravity power is expressed as follows

$$\dot{W}_4 = \omega\gamma\sum_{j=1}^{n}\int_{\theta_{j-1}}^{\theta_j}\int_o^r \rho^2\cos(\beta+\theta)d\rho d\theta, \tag{27}$$

where ω is the angular velocity of the rotation of the plastic zone BCD around point B. The rate of the rigid body BDE weight takes the form

$$\dot{W}_5 = -\omega\gamma S_{BDE} r_n \cos(\pi-\beta-\theta_a), \tag{28}$$

$$S_{BDE} = \frac{1}{2}r_n^2 \frac{\sin(\beta+\theta_a)\cos\varphi_n}{\cos(\pi-\beta-\theta_a+\varphi_n)}, \tag{29}$$

where r_n is expressed in Eq. (11). The dissipation of internal energy on the speed discontinuity line BC is expressed as follows

$$v_{CB} = v_0 \frac{\sin\beta}{\cos(\beta-\varphi_1)}, \tag{30}$$

$$\dot{D}_1 = \omega(\tau_1 - \sigma_{n1}\tan\varphi_1) r_0^2 \frac{\sin\beta\cos\varphi_1}{\cos(\beta-\varphi_1)}. \tag{31}$$

The integrated power dissipation rate for all n segments in the rupture surface $C_0C_jC_n$ is the same as the energy dissipation inside the plastic zone BCD, expressed as follows

$$\dot{D}_2 = 2\omega\sum_{j=1}^{n}\int_{\theta_{j-1}}^{\theta_j}(\tau_j - \sigma_{nj}\tan\varphi_j) r^2\, d\theta, \tag{32}$$

where τ_j and σ_{nj} are the shear and normal stress in soil at different damage locations (Fig. 1(b)), respectively. φ_j is the failure angle of part j in BCD of the plastic zone, and r is presented in Eq. (10). The dissipation of internal energy on the line DE is expressed as follows

$$\dot{D}_3 = \omega(\tau_n - \sigma_{nn}\tan\varphi_n) l_{DE} r_n \cos\varphi_n, \tag{33}$$

$$l_{DE} = \frac{r_n\sin(\beta+\theta_a)}{\cos(\pi-\beta-\theta_a+\varphi_n)}. \tag{34}$$

Finally, according to Eq. (21), the upper limit solution of strip footing can be calculated, which is expressed as Eq. (35). Because the rupture angles of the failure mechanisms used are different, N_c cannot be put forward like the Terzaghi formula, so N_c' is used in this paper.

$$p = \frac{1}{2}\gamma b N_r + qN_q + N_c', \tag{35}$$

$$q = \gamma d, \tag{36}$$

where d is the foundation buried depth. The formulas of the coefficients in Eq. (35) and the calculation process will be described in detail in Appendix A.

3.2.2 Unilateral Failure Mechanism

The formulations for internal energy dissipation of the failure mechanism considering seismic forces are as follows:

$$\dot{D}_{\text{int}} = \dot{D}_{\text{AC}} + \dot{D}_{\text{CD}} + \dot{D}_{\text{DE}} + \dot{D}_{\text{BCD}}, \tag{37}$$

$$\dot{D}_{\text{AC}} = \omega r_0 b \sin\beta f_1, \tag{38}$$

$$\dot{D}_{\text{DE}} = \omega r_n^2 f_2, \tag{39}$$

$$\dot{D}_{\text{CD}} = \dot{D}_{\text{BCD}} = \omega\sum_{j=1}^{n}\int_{\theta_{j-1}}^{\theta_j}(\tau_j - \sigma_{nj}\tan\varphi_j) r^2\, d\theta. \tag{40}$$

The work done by external forces is divided as follows: the work done by load P of the foundation $\dot{W}_P$, the work done by stacking load q $\dot{W}_q$, the work done by soil gravity $\dot{W}_G$, and the work done by seismic forces $\dot{W}_s$, which are shown as follows:

$$\dot{W}_{\text{ext}} = \dot{W}_P + \dot{W}_q + \dot{W}_G + \dot{W}_s, \tag{41}$$

$$\dot{W}_P = \omega r_0 b P f_3, \tag{42}$$

$$\dot{W}_q = \omega r_n^2 q f_4, \tag{43}$$

$$\dot{W}_G = \omega\gamma f_5. \tag{44}$$

The work done by seismic forces is calculated using the slice

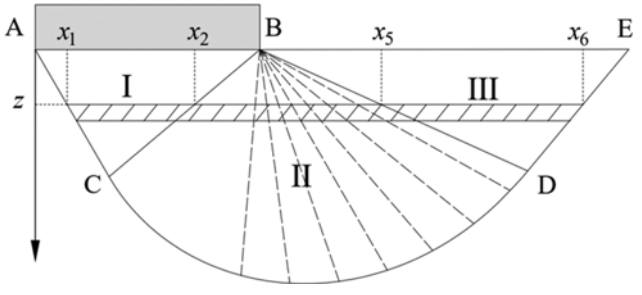

Fig. 6. The Diagram of the Slice Integration Approach for Regions I and III

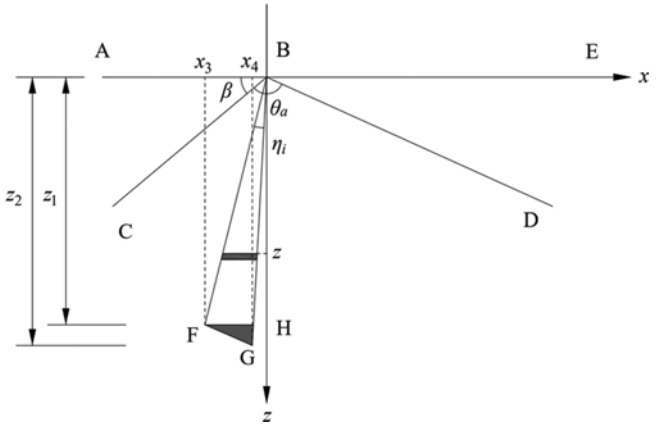

Fig. 7. The Details of the Slice Integration Approach for Region II

integration method and divided into three parts (Liu et al., 2022), as shown in Figs. 6 and 7. The calculation of the plastic zone is complicated, in order to simplify the calculation, the piece-wise logarithmic spiral of the plastic zone is simplified to some straight lines and the velocity on the same horizontal plane is assumed to be constant. The calculation formula is shown as follows:

$$\dot{W}_s = \dot{W}_{s1} + \dot{W}_{s2} + \dot{W}_{s3} \tag{45}$$

$$\dot{W}_{s1} = \int_0^{\bar{z}_c} \gamma v_0 \sin\beta k_h(z, t)(x_2 - x_1)dz = \omega k_h \gamma r_0 b^2 \sin\beta f_6\,, \tag{46}$$

$$\dot{W}_{s3} = \int_0^{\bar{z}_D} \gamma v_n \sin(\beta + \theta_a) k_h(z, t)(x_6 - x_5)dz = \omega k_h \gamma r_0 b^2 \sin(\beta + \theta_a) e^{\sum_{i=1}^{n} \eta_i \tan\varphi_i} f_7\,, \tag{47}$$

$$\dot{W}_{s2} = \sum_{i=0}^{n-1} (d\dot{W}_{s2.1} + d\dot{W}_{s2.2})\,, \tag{48}$$

$$d\dot{W}_{s2.1} = \int_0^{\bar{z}_1} \gamma v_{ih} k_h(z, t)(x_4 - x_4)dz = \omega k_h \gamma r_0 b^2 f_8 f_9\,, \tag{49}$$

$$d\dot{W}_{s2.2} = \frac{1}{2}\omega\gamma z_1(z_2 - z_1) r_0 k_h(z_1, t) f_8\,. \tag{50}$$

The formula of the bearing capacity is calculated by carrying the above results into Eq. (21), and it is expressed as Eq. (51). Additional details are shown in the Appendix B.

$$p_e = \frac{1}{2}\gamma b N_{re} + q N_{qe} + N'_{ce} \tag{51}$$

4. Calculation Results and Discussions

The paper is dedicated to the assessment of the bearing capacity of strip footings on c and φ soils that obeying the nonlinear MC criterion. Using the GA (genetic algorithm), the minimum upper bound of the foundation bearing capacity was computed by optimizing the geometric parameters β, θ_a, η_i, (time parameter t) and rupture angle φ_i through continuous iteration. Genetic algorithms model the genetic behavior of biological genes. After forming an initial population by coding, the task of genetic manipulation is to impose certain operations on the individuals of the population according to their adaptation to the environment, thus realizing the evolutionary process of survival of the fittest. In terms of optimized search, genetic operations allow the solution of a problem, generation after generation, to be optimized and approximate the optimal solution. Fig. 8 illustrates the operational steps of the GA.

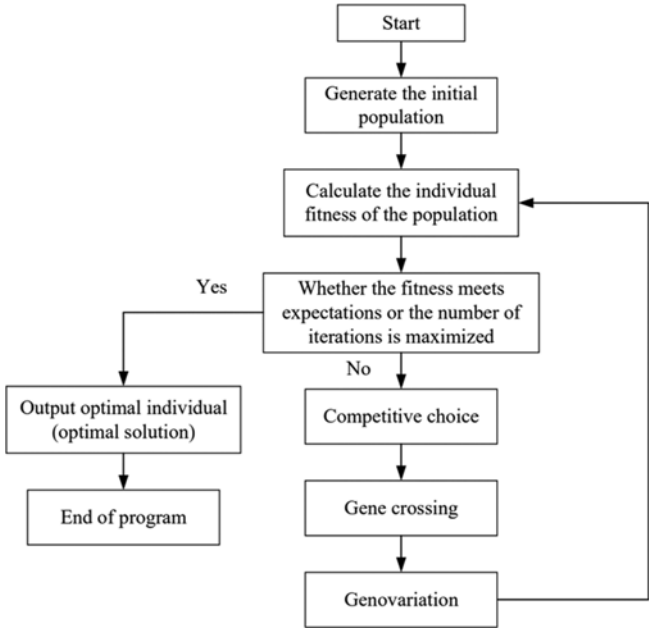

Fig. 8. The Flowchart of Genetic Algorithm Concept

According to Coley (1999), within the given range of parameter values, after continuous attempts, the specific parameters of the GA (genetic algorithm) are set as follows:

'PopulationSize' is 100, 'CrossoverFraction' is 0.8, 'MigrationFraction' is 0.01, 'Generations' is 100 times the number of variables. In addition, 'TolFun' is $1 \times e^{-6}$. It means that when the difference between the results of two successive calculations was less than 10^{-6}, the iteration was terminated. Based on the above parameters settings, the result is obtained after continuous iterative optimization.

4.1 No Consideration of Seismic Effects

4.1.1 Astringency

The first problem in employing the bearing capacity formulation in Eq. (35) is the determination of the optimal value of n in the plastic zone BCD. Each part has a separate and uncertain rupture angle φ in the plastic zone BCD, and the precision of calculations improves as the number of parts n grows. But as n increases, the computation time increases, while the change in the result is negligible when n reaches a certain value. From Table 1, the accuracy of the computation results did not improve obviously as the number of sectors continues to increase when n is more than 8. Therefore, after calculation and comparison, the number of

Table 1. p Values Versus the Number of Segments n (kPa)

	n											
c_0	1	2	3	4	5	6	7	8	9	10	11	12
150	3581.6	3435.1	3413.3	3406.7	3404.0	3402.7	3401.9	3401.5	3400.3	3400.1	3399.0	3398.7
180	5557.6	5225.6	5176.2	5161.3	5155.2	5152.1	5150.4	5149.3	5147.0	5145.4	5144.4	5144.3

γ = 19 kN/m^3, σ_t =247.3 kPa, m = 1.2, d = 3 m, and b = 2 m. (The unit of c_0 is kPa)

Table 2. The Comparison of Bearing Capacity under Different n Conditions (kPa)

	Nonlinear parameter m							
c_0	1.2	1.2	1.4	1.4	1.6	1.6	1.8	1.8
	$n = 1$	$n = 8$	$n = 1$	$n = 8$	$n = 1$	$n = 8$	$n = 1$	$n = 8$
60	694.92	690.30	613.66	609.10	564.39	560.41	531.38	527.95
90	1302.85	1281.31	1074.78	1056.41	948.23	933.59	868.23	856.37
120	2221.72	2152.50	1701.78	1650.53	1437.75	1400.27	1279.96	1251.28
150	3581.57	3401.45	2534.54	2418.33	2047.98	1969.62	1772.63	1715.76
180	5557.60	5149.27	3618.81	3388.38	2794.41	2650.56	2352.01	2252.65

γ=19 kN/m^3, σ_t =247.3 kPa, d = 3 m, and b = 2 m.

Table 3. Parameter Values for Different Soils

Soils	γ(kN/m^3)	MC failure criterion			Nonlinear MC failure criterion		
		m	c (kPa)	σ_0 (kPa)	m	c (kPa)	σ_0 (kPa)
[a]London clay	18.0	1.0	6.0	9.602	1.66	1.05	0.15
[b]Nigeria clay	18.0	1.0	29.40	76.990	1.34	0.54	0.168
[c]Toyoura sand (Dr = 60%)	14.81	1.0	3.040	3.877	1.16	3.34×10^{-3}	0.806×10^{-3}
[c]Toyoura sand (Dr = 90%)	15.79	1.0	3.040	3.294	1.16	3.62×10^{-3}	0.743×10^{-3}

[a]Parameter values from the paper of Baker (2004).
[b]Parameter values from the paper of Anyaegbunam (2015).
[c]Parameter values from the paper of Serrano et al. (2016) and Kobayashi et al. (2009).

Table 4. A Comparison of Bearing Capacity p (kPa)

	Ganesh and Kumar (2021)						Present study		
	MC failure criterion			Nonlinear MC failure criterion			Nonlinear MC failure criterion		
	b = 1.0 m	b = 2.0 m	b = 5.0 m	b = 1.0 m	b = 2.0 m	b = 5.0 m	b = 1.0 m	b = 2.0 m	b = 5.0 m
London clay	483.82	709.83	1335.3	254.15	292.16	364.55	261.73	299.54	374.54
Nigeria clay	526.88	584.39	736.33	347.87	438.33	614.54	362.40	460.04	653.06

Table 5. A Comparison of Bearing Capacity p (kPa)

	Chen et al. (2022)						Present study		
	MC failure criterion			Nonlinear MC failure criterion			Nonlinear MC failure criterion		
	b = 1.0 m	b = 2.0 m	b = 5.0 m	b = 1.0 m	b = 2.0 m	b = 5.0 m	b = 1.0 m	b = 2.0 m	b = 5.0 m
London clay	504.86	731.74	1399.78	305.62	342.06	415.89	261.73	299.54	374.54

sectors, n, was determined as 8. Comparing the results for n = 8 to for n = 1 in Table 2, the average difference is around 5%. False convergence may occur when using the optimization algorithm, in which the results fluctuate with increasing values of the parameters. However, it can be found from Table 1 that there is an extremely strong astringency on the bearing capacity as n increases. This fact initially confirms the feasibility of the approach in this paper. In addition, to compare optimization results more significantly, partial results of the calculations are presented.

4.1.2 Comparisons

In the existing literature on assessing the bearing capacity, a small amount of literature used the nonlinear MC failure criterion, but the authors note that most of them use the single tangent method. To estimate the feasibility of the approach in the paper, some data results are presented and compared with Ganesh and Kumar (2021) and Chen et al. (2022). Ganesh and Kumar (2021) calculated the bearing capacity of foundations of different cross-sections resting on soils conforming to the nonlinear MC criterion by employing the stress characteristics approach, and the parameters of the soil are written in Table 3. Following the nonlinear MC failure criterion, Chen et al. (2022) evaluated the bearing capacity of foundations by adopting the single tangent method.

The comparisons are listed in Tables 4 – 6. It can be found that most of the results in this paper are closer to the results of

Table 6. A Comparison of Bearing Capacity p (kPa) with b = 0.02 m

	Dr	Kobayashi et al. (2009)	Ganesh and Kumar (2021)		Present study
			Mohr-Coulomb failure criterion	Nonlinear MC failure criterion	
Toyoura sand	60%	71.27 – 108.24	204.71	120.25	140.64
Toyoura sand	90%	113.14 – 183.52	349.23	240.45	323.57

Ganesh and Kumar (2021), and the average difference is about 3%. Only the results of Toyoura sand where Dr = 90% are larger. However, compared with Chen et al. (2022), the results in this paper are significantly smaller, and that's a reduction of about 15%. It can be found that there is a large difference between the nonlinear solutions of Chen et al. (2022) and Ganesh and Kumar (2021) by comparison, and Chen et al. (2022) explains that the single tangent approach is adopted. However, the results in the paper are similar to those of Ganesh and Kumar (2021). Therefore, the above comparisons prove the effectiveness of the method in the paper, and compared with the single tangent approach, a more accurate upper bound solution is obtained.

4.1.3 Effect of Nonlinear Failure Criterion Parameters

Select nonlinear failure criterion parameters: c_0 = 90 kPa, σ_t = 247.3 kPa. The bearing capacity and its correlation coefficients are presented in Fig. 8 through the optimization calculation. From Fig. 9, the ultimate bearing capacity and coefficients both decrease with the increase of m. when $m > 3$, N_γ is close to zero, so the effect of soil weight can be neglected. In addition, it can be noted that $m = 2$ is a roughly turning point, after which the curves become flat. It is not possible to treat the cohesion c as a factor using the method presented in this paper. Therefore, N_c' is used to represent the contribution of cohesion c to the bearing capacity and presented in Fig. 9(d). As m increases, N_c' decreases and stabilizes gradually. It can be obviously found that when m is large enough, the contribution of N_c' to the bearing capacity accounts for the major part.

Because the limitation of test conditions, it is difficult to accurately measure cohesion at zero normal stress c_0 and uniaxial

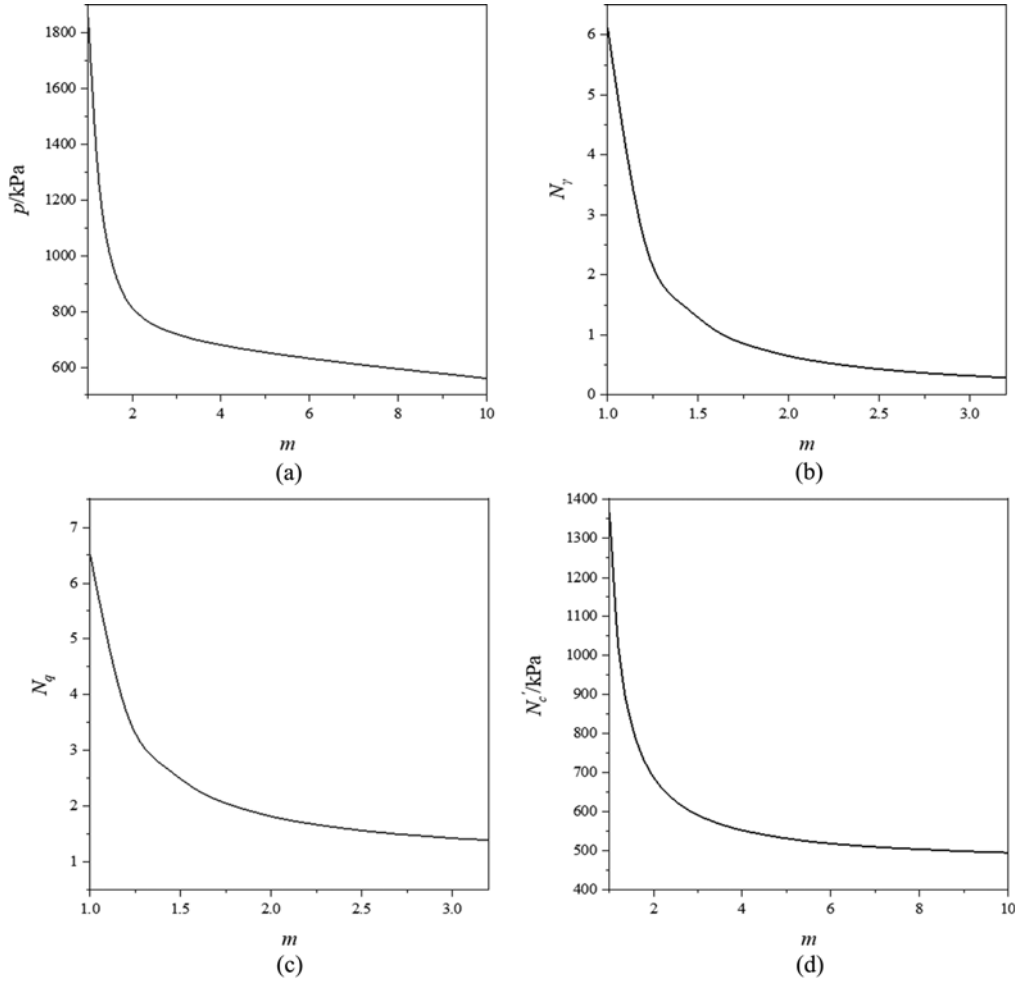

Fig. 9. Effect of Nonlinear Parameter m on Ultimate Bearing Capacity: (a) p, (b) N_γ, (c) N_q, (d) N_c'

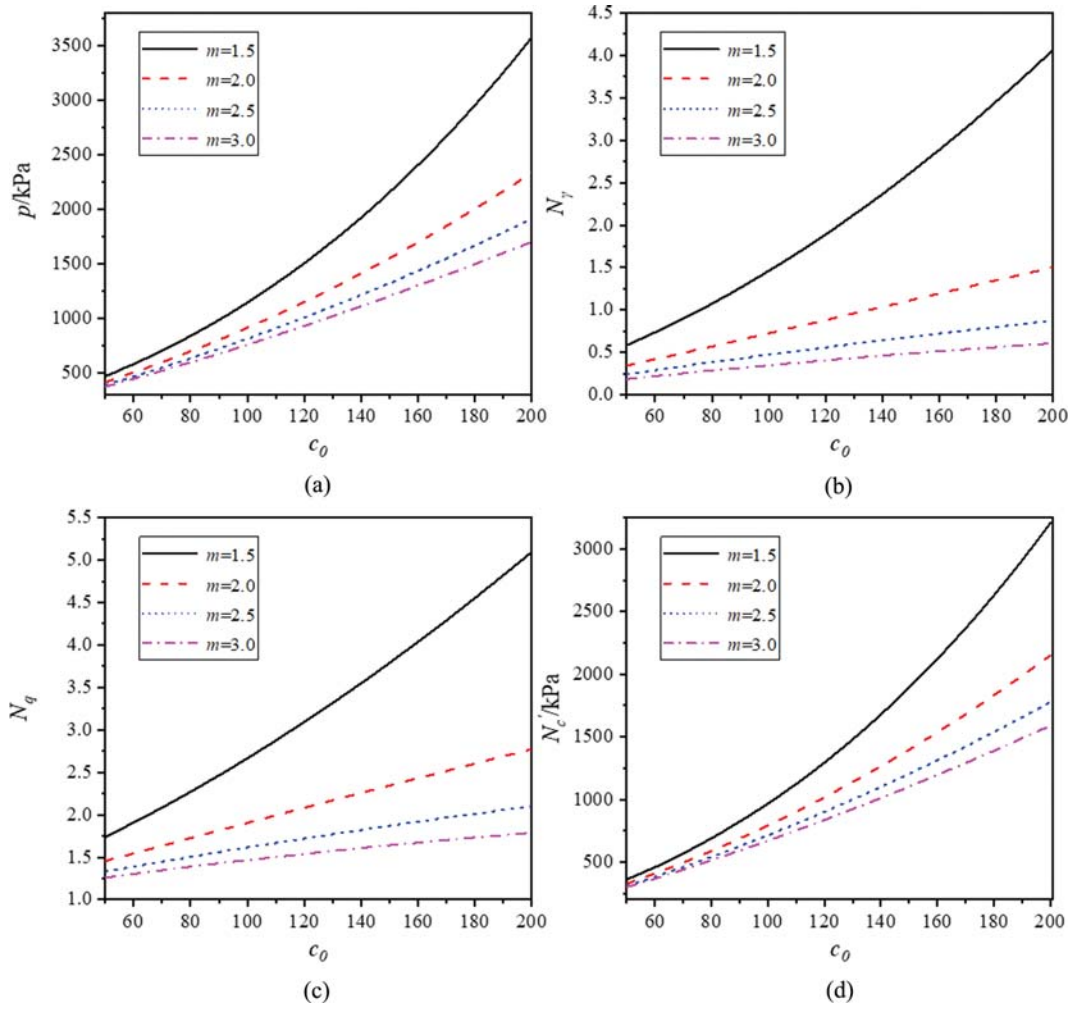

Fig. 10. Effect of the Cohesion at Zero Normal Stress c_0 on Ultimate Bearing Capacity: (a) p, (b) N_γ, (c) N_q, (d) N_c'

tensile stress σ_t for some soil bodies. It is essential to explore its influence on the bearing capacity calculation. From Fig. 10, the bearing capacity and its coefficients both increase as c_0 increases. When c_0 is small, the bearing capacity and its coefficients are almost equal for taking different values of m, and as c_0 increases, the gap becomes gradually obvious. Obviously, the larger the value of m, the smoother the bearing capacity and its coefficients curve.

From Fig. 11, the bearing capacity and its coefficients decrease with the increase of uniaxial tensile stress σ_t. When uniaxial tensile stress σ_t is larger, the gap between curves with different values of m is smaller until it is stable. As m increases, the difference between the bearing capacity and its coefficients gradually decreases for the same m gap. When m is large, N_γ tends to 0, and it means that the effect of the soil weight can be ignored. It can be seen from the comparison of Figs. 10 and 11 that the influences of c_0 and σ_t on the ultimate bearing capacity are completely opposite.

The above analysis reveals that the selection of suitable nonlinear parameters is essential for the accurate assessment of bearing capacity.

4.2 Consideration of Seismic Effects

Earthquakes are one of the common natural disasters that cause engineering problems worldwide. Therefore, it is necessary to consider the influences of seismic action in earthquake-prone areas. Many analyses have shown that seismic action reduces the foundation bearing capacity. The pseudostatic approach is employed widely. However, the pseudostatic approach does not take into account the dynamic response of seismic action, which has a non-negligible shortcoming. Some scholars adopted the pseudo-dynamic approach to evaluate the seismic bearing capacity of foundation (Ghosh, 2008; Zhong et al., 2022; Chen et al., 2022), but the approach also has some limitations, it does not consider the damping ratio of geotechnical materials and the boundary conditions of free surface. Therefore, a modified unilateral failure mechanism was established in this paper, and the effect of seismic was studied employing a modified pseudo-dynamic method.

Previous literature studies have shown that the influence of vertical soil acceleration on the seismic response of the system is negligible (Gazetas et al., 2004; Huang, 2005). Therefore, only the influence of horizontal seismic forces is considered in the paper.

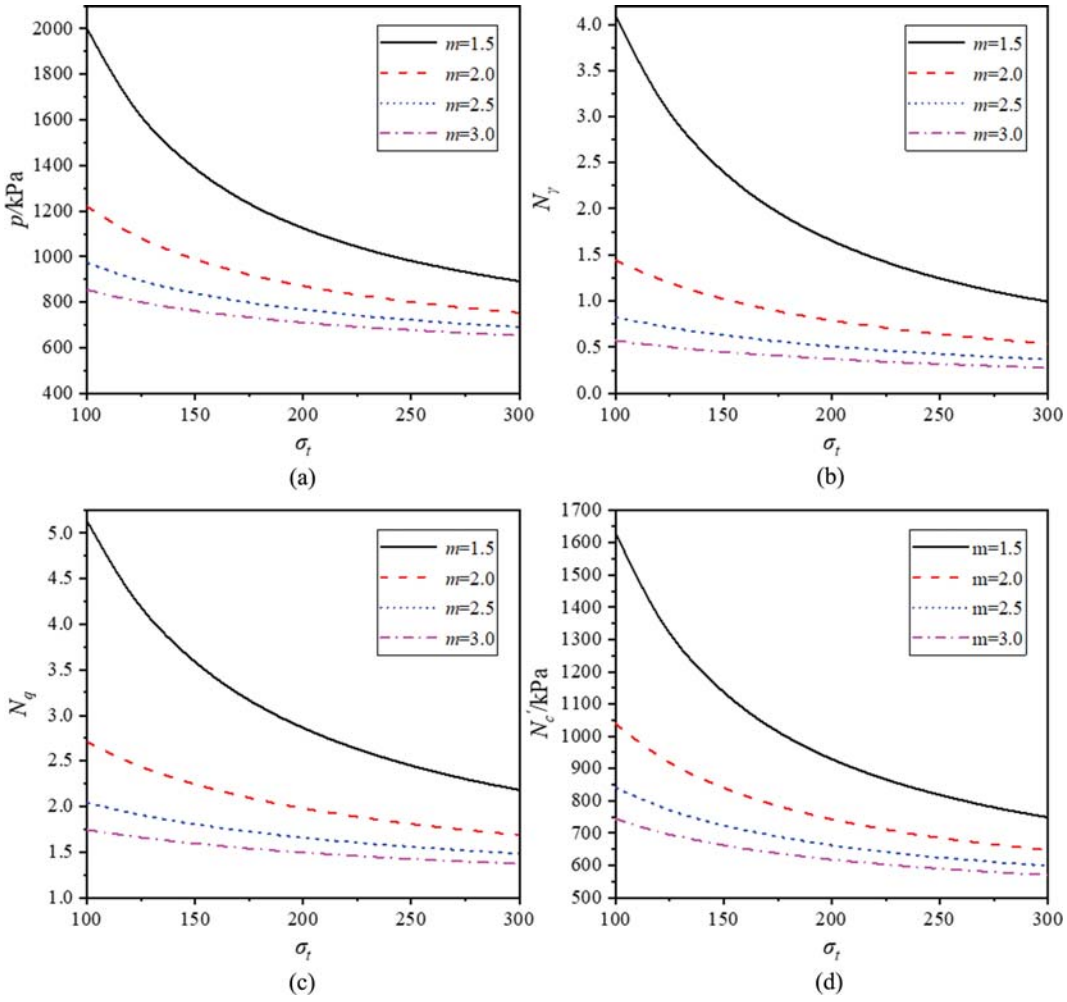

Fig. 11. Effect of Uniaxial Tensile Stress σ_t on Ultimate Bearing Capacity: (a) p, (b) N_γ, (c) N_q, (d) N_c

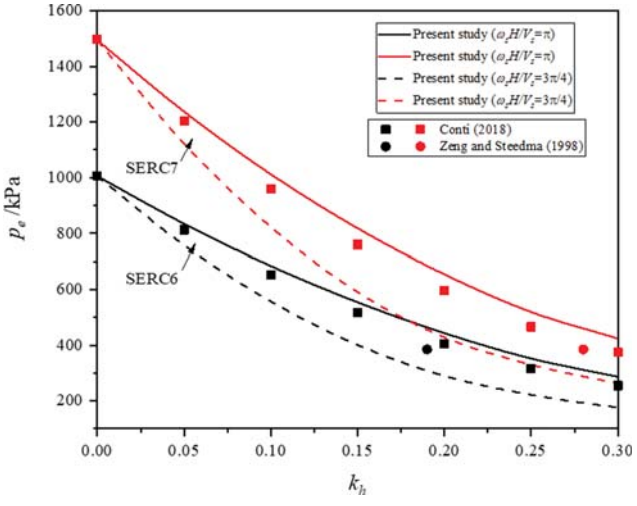

Fig. 12. Comparison with Results from Other Literature

4.2.1 Comparisons

In order to verify the validity of the results of this paper, the results were compared with those of other literature. When m = 1, the nonlinear MC criterion becomes the linear MC criterion, and the results of this paper are compared with the experimental results of Conti (2018) and Zeng and Steedma (1998) at m = 1 as well as n = 1, as shown in Fig. 12. Taking two different sandy soils as an example, the parameters are selected as follows: b = 1.67 m, d = 0.5 m (SERC6: γ = 5.5 kN/m^3, φ = 41°; SERC7: γ = 6.3 kN/m^3, φ = 42.4°). When $\omega_s H/V_s = \pi$, the results of this paper are slightly larger than those of Conti (2018) and Zeng and Steedma (1998), while the opposite results are presented for $\omega_s H/V_s = 3\pi/4$. It can be seen that $\omega_s H/V_s$ has a greater influence on the seismic bearing capacity of the foundation. In addition, Fig. 13 illustrates a comparison of the bearing capacity using different methods, where $\lambda = TV_s$. The results using the modified pseudo-dynamics method and the results using the spectral pseudo-dynamics method has a similar regularity. The differences of results may be due to the use of different methods as well as different failure mechanisms. It can be seen that the bearing capacity reaches its minimum at λ/H = 4 ($\omega_s H/V_s = \pi/2$), which is caused by a sudden increase in the seismic acceleration coefficient at this case. Fig. 14 compares the seismic acceleration coefficients $k_h(z, t)$ at $\omega_s H/V_s = \pi/2$ and $\omega_s H/V_s = \pi$. The coefficient of seismic acceleration at the soil surface when $\omega_s H/V_s = \pi/2$ increases by a

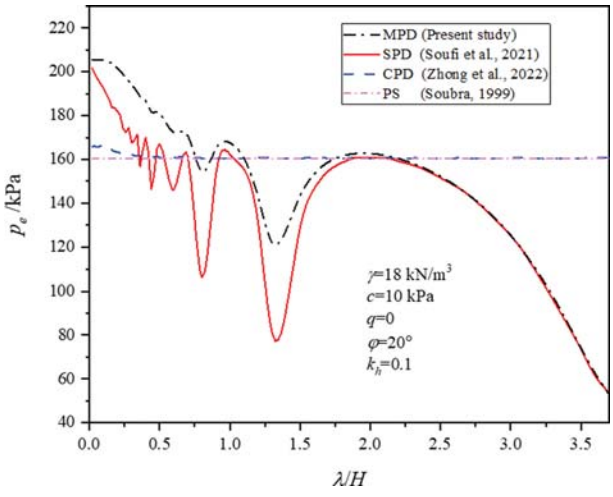

Fig. 13. Comparison of Results Using Different Methods

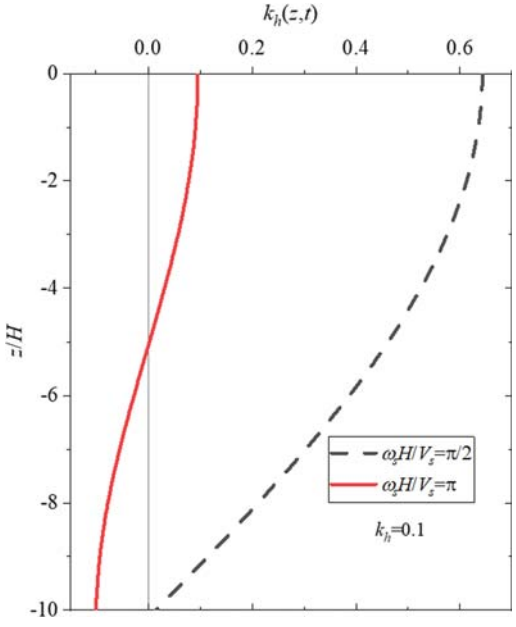

Fig. 14. Comparison of $k_h(z, t)$ for Different $\omega_s H/V_s$

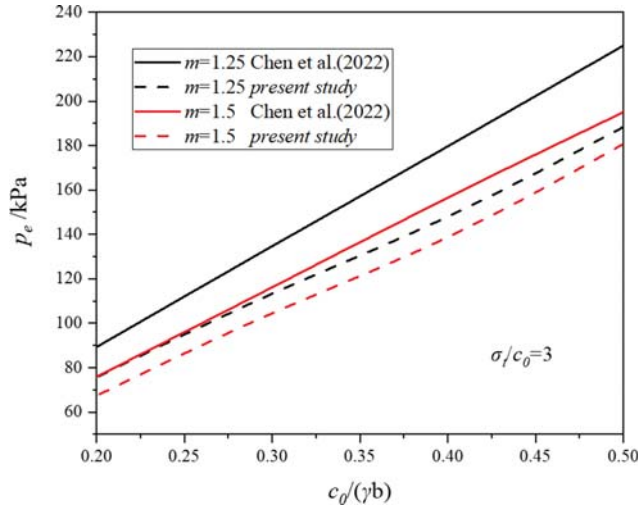

Fig. 15. Comparison of Bearing Capacity for Different Parameter Values

factor of about 5 compared to the result when $\omega_s H/V_s = \pi$. Therefore, the bearing capacity of the foundation is lower in this case.

In addition, the results are compared with those of Chen et al. (2022), as shown in Fig. 15. The soil parameters are selected as $b = 3$ m, $d = 0$ m, $\gamma = 18$ kN/m^3, $k_h = 0.2$, $\omega_s H/V_s = \pi/2$, and $H = 3$ m. The ultimate bearing capacity obtained in this paper is reduced by about 15% in the case of $m = 1.25$ and by about 7% in the case of $m = 1.5$, compared with the results of Chen et al. (2022). The authors believe that there are two reasons for getting smaller bearing capacity values in this paper, one is the piecewise method used in this paper, and the other is the MPD approach considers the effect of normalized frequency $\omega_s H/V_s$.

4.2.2 Effect of Nonlinear Failure Criterion Parameters

The soil parameters are selected as $b = 1$ m, $d = 0$ m, $\gamma = 18$ kN/m^3, $c_0 = 90$ kPa, $\sigma_t = 247.3$ kPa, $k_h = 0.1$, $\omega_s H/V_s = \frac{\pi}{4}$. From Fig.

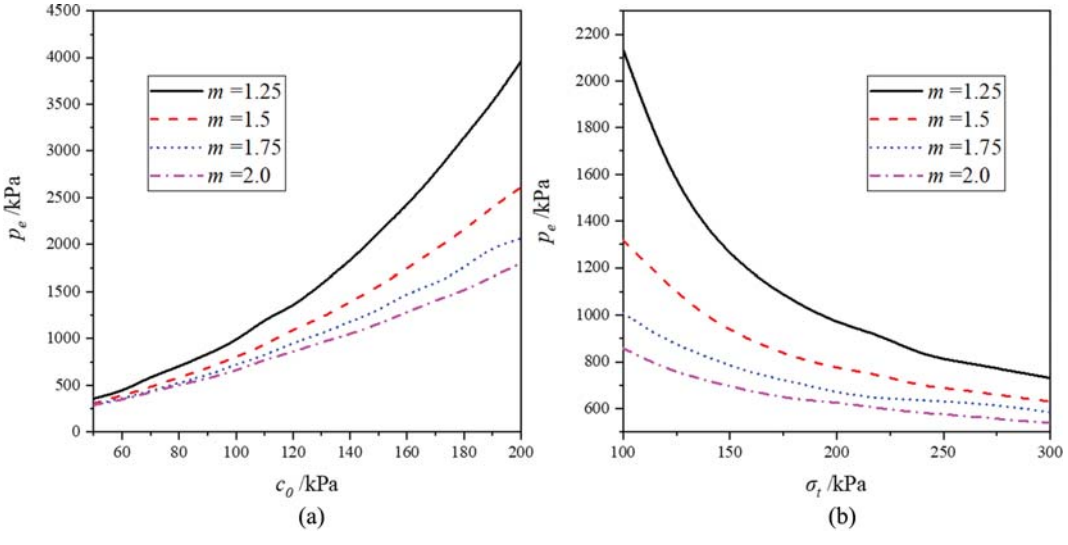

Fig. 16. Influence of the Nonlinear Failure Criterion Parameters: (a) c_0, (b) σ_t

16, it can be found that the influence of nonlinear parameters on the seismic bearing capacity is similar to that on the static bearing capacity. p_e increases with the increase of c_0 and decreases with the increase of m and σ_t. As m increases from 1.25 to 2.0, the seismic bearing capacity p_e will decrease by about 50% at most. The degree of influence of c_0 and σ_t on the seismic bearing capacity p_e also has a great relationship with m. The smaller the m, the more significant the effect of c_0 and σ_t. The influence of c_0 on the seismic bearing capacity is greater than the effect of σ_t. c_0 decreases from 200 to 50, p_e decreases up to 90%, and σ_t increases from 100 to 300, p_e decreases up to 70%. Therefore, the selection of nonlinear parameters has a key role in the accurate assessment of the seismic bearing capacity.

4.2.3 Effect of MPD Parameters

In the paper, the influence of MPD parameters is shown in Figs. 17 and 18. Fig. 17 illustrates that the seismic bearing capacity p_e decreases with the increase of k_h for different m, and the effect of k_h on p_e decreases as m becomes larger. Fig. 18 depicts the effect of the normalized frequency $\omega_s H/V_s$ and the damping ratio ξ. As the damping ratio ξ increases, p_e also increases. When $\omega_s H/V_s = \frac{\pi}{2}$, there is a clear trough in p_e, and the highest point of p_e differs from the lowest point by about 27% at most.

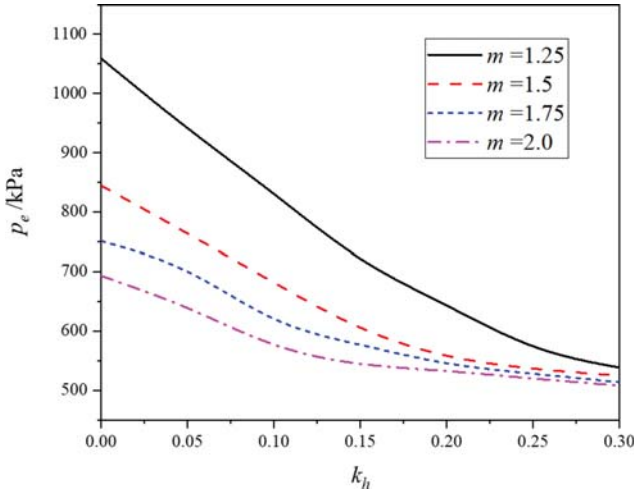

Fig. 17. The Variation of p_e with k_h in the Case of Different m

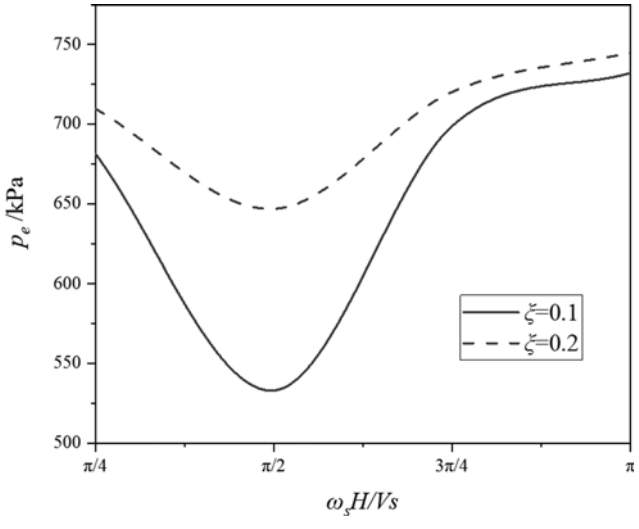

Fig. 18. The Variation of p_e with $\omega_s H/V_s$ in the Case of Different ξ

Therefore, the damping ratio ξ and the normalized frequency $\omega_s H/V_s$ have a large influence on the assessment of the seismic bearing capacity, while the traditional pseudo-static approach and pseudo-dynamic method are unable to consider these factors and have certain limitations. This also confirms the merits and feasibility of the method in this paper.

4.3 Discussion and Analysis

The linearization of the nonlinear MC criterion or the HB criterion is used extensively in the bearing capacity calculation of geotechnical foundations. For bearing capacity calculation of foundations, the single tangent or multi-tangent method is a single-sided improvement on the use of the nonlinear MC criterion. The approach presented in the paper shown that study can be performed without compromising the failure envelope's real nonlinear pressure dependency.

The BCD region was viewed as a whole rotating with angular velocity w in the modified failure mechanism, and the BCD region was divided into sectors with separate rupture angles φ_i, which gives geometric flexibility to the mechanism so that the optimal upper bound to the ultimate bearing capacity could be obtained. The sectors' corresponding angle was discovered during the optimization process, rather than being predetermined. The rupture surface is not strictly smooth. Nonetheless, as the number of sectors n grows, it will approximate a smooth curve. By comparison, n was chosen to be 8. A larger n does not significantly improve the calculation accuracy. Then the selection of the nonlinear parameters and the influence of seismic forces are studied. The data indicate that a more accurate solution is obtained considering the modified failure mechanism and the piece-wise method.

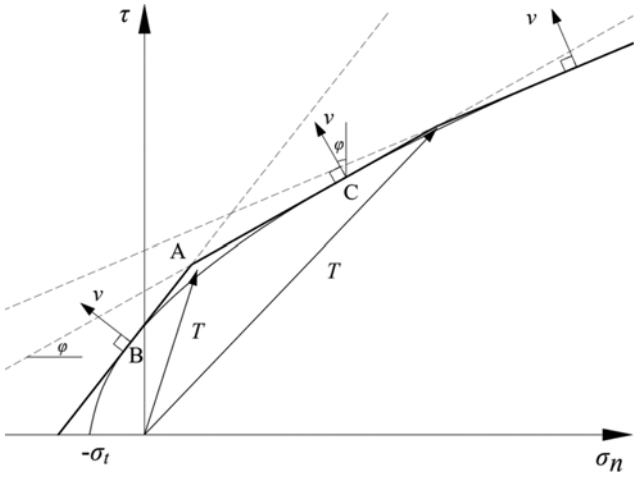

Fig. 19. The Case of an Impermissible Stress Vector for a Piece-Wise Linear Failure Envelope

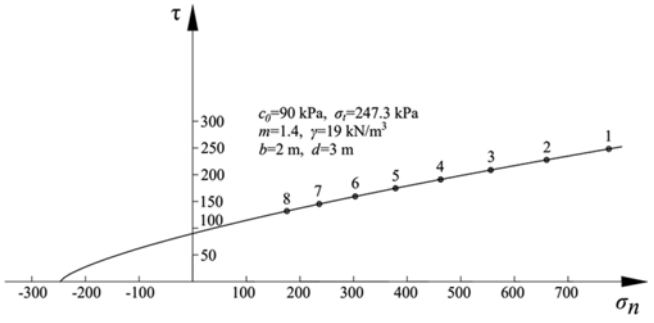

Fig. 20. Stress on the Failure Surface Mapped on the Nonlinear MC Failure Envelope

The essence of the single tangent approach is to approximate the soil as a linear failure material, to calculate its ultimate bearing capacity. A similar explanation is not suitable for the piece-wise log-spiral failure mechanism, since it would mean that the failure envelope of the soil body on the plane τ, σ_n is piece-wise linear. In the above envelope, there may be stress vectors that are not allowed. For example, the stress vector T pointing to the ABC range in Fig. 19 is the one that crosses the envelope boundary.

In the proposed failure mechanism, the stress vector follows the surface $C_0C_fC_n$ is distributed in multiple segments, and the rupture angle of each sector corresponds to a point on the failure criterion. The approach can be interpreted as the stress vector along the whole surface $C_0C_fC_n$ is characterize by scattered points on the failure envelope, for instance, the eight spots illustrated as black circles in Fig. 20 for $n = 8$. Such a stress field is unbalanced, but the stress fields constructed by the kinematic analysis are not required to be equalized. Although the stress vector produced thusly is not the genuine stress, from another point of view, the trend of the solutions can be seen by observing the obtained stress data on the rupture surface. From the stress distribution in Fig. 20, it can be found that the failure of the soil presents a nonlinear situation. Taking the right half of the mechanism as an example, the normal stress decreases gradually from left to right on the rupture surface, which is more in accordance with the real state of soil damage. When the bearing capacity is evaluated following the linear MC criterion, there is no doubt that a large upper bound solution will be obtained. Therefore, the piece-wise approach based on the proposed specific failure mechanism in this study is different from the single tangent method or multi-tangent method. The calculated ultimate bearing capacity in this paper is a strict upper limit solution, for the soil that follow the nonlinear MC criterion without the used linear approximation.

5. Conclusions

Numerous studies have shown that nonlinear failure is closer to the true situation of soil strength. Therefore, based on the modified failure mechanism, the upper bound approach of limit analysis was used for c and φ soil that are restricted by the nonlinear MC criterion, and the static and seismic bearing capacity of foundations was calculated by using the GA in this paper.

Two types of piece-wise log-spiral failure mechanisms for bearing capacity estimation are proposed in this paper, where the rotating plastic zone BCD was separated into sectors with varying rupture angles. The distribution of the stress vector on the surface $C_0C_fC_n$ is reflected by different rupture angles on the failure envelope. Based on the symmetrical failure mechanism, the bearing capacity of foundations under static condition was studied. And following the unilateral failure mechanism, the seismic bearing capacity of the foundation was evaluated using the modified pseudo-dynamic approach. To illustrate the significance of the work in this paper, the comparisons with other literature data was made and the parametric analysis was performed, with the following main conclusions:

1. The bearing capacity values using the nonlinear MC criterion are significantly lower than those using the linear MC criterion. In addition, compared with the single tangent approach, a more accurate upper bound solution is obviously obtained using the method of the paper, which confirms that the method of the paper is more suitable for the nonlinear failure criterion.
2. The parameters of the nonlinear MC criterion have a significant effect on the bearing capacity of foundations. The bearing capacity decreases rapidly when the nonlinear parameter m increases from 1 to 3, and slows down when m is greater than 3. Similarly, the bearing capacity tends to decrease with increasing σ_t. However, as c_0 increases, the bearing capacity gradually increases.
3. Compared to the pseudo-static method and the conventional pseudo-dynamic method, the modified pseudo-dynamic method takes into account the effects of damping ξ as well as normalized frequency $\omega_s H/V_s$. By parametric analysis, both ξ and $\omega_s H/V_s$ have a non-negligible effect on the seismic bearing capacity of foundations, and when the normalized frequency $\omega_s H/V_s$ is equal to $\frac{\pi}{2} + n\pi (n = 0, 1, 2\cdots)$, the seismic bearing capacity of foundations will be significantly reduced.

This paper gives a theoretical basis for the calculation of the seismic bearing capacity of foundations based on the nonlinear MC criterion. However, there are some limitations. This study did not consider the effects of variation in moisture as well as variation in temperature. This direction should be explored in future work. In addition, the work can be further extended by, for example, considering transient flow, three-dimensional failure mechanism for foundations.

Acknowledgments

Not Applicable

Nomenclature

b = Width of the foundation
c = Cohesion

c_0 = Cohesion at zero normal stress
d = Overburden thickness
$\dot{D}_{\text{int}}$ = The power of the internal force
g = Acceleration of gravity
H = The depth to bedrock
k_h = Initial factor of seismic acceleration
m = Nonlinear parameter
n = Number of logarithmic spiral areas
N_c' = Static parameter related to soil cohesion
N_{ce}' = Seismic parameter related to soil cohesion
N_q = Static parameter related to uniform load
N_{qe} = Seismic parameter related to uniform load
N_γ = Static parameter related to soil unit weight
$N_{\gamma e}$ = Seismic parameter related to soil unit weight
p = Static bearing capacity of the foundation
p_e = Seismic bearing capacity of the foundation
q = Uniform load
r_i = The line BC_i
t = Time parameter
v_i = velocity of the ith part
V_s = Velocity of the shear wave
$\dot{W}_{\text{int}}$ = the power of the external force
y_1 = Constant
z = Depth below ground surface
β = Angle between line BA and line BC
η_i = Top corner of part i
γ = Unit weight of soil
φ = Internal friction angle
φ_i = Rupture angle of the ith part
θ_a = Angle between line BC and line BD
σ_n = Normal stress
σ_t = Tensile stress
τ = Shear stress
ξ = Damping ratio
ω = Angular velocity of failure mechanism
ω_s = Angular frequency
ψ_2 = Constant

ORCID

Not Applicable

References

AlKhafaji H, Imani M, Fahimifar A (2020) Ultimate bearing capacity of rock mass foundations subjected to seepage forces using modified Hoek-Brown criterion. *Rock Mechanics and Rock Engineering* 53(1):251-268, DOI: 10.1007/s00603-019-01905-6

Anyaegbunam AJ (2015) Nonlinear power-type failure laws for geomaterials: Synthesis from triaxial data, properties, and applications. *International Journal of Geomechanics* 15(1):04014036, DOI: 10.1061/(ASCE)GM.1943-5622.0000348

Baker R (2004) Nonlinear Mohr envelopes based on triaxial data. *Journal of Geotechnical and Geoenvironmental Engineering* 130(5):498-506, DOI: 10.1061/(ASCE)1090-0241(2004)130:5(498)

Bellezza I (2014) A new pseudo-dynamic approach for seismic active soil thrust. *Geotechnical and Geological Engineering* 32:561-576, DOI: 10.1007/s10706-014-9734-y

Beygi M, Vali R, Keshavarz A (2022) Pseudo-static bearing capacity of strip footing with vertical skirts resting on cohesionless slopes by finite element limit analysis. *Geomechanics and Geoengineering* 17(2):485-498, DOI: 10.1080/17486025.2020.1794058

Cascone E, Casablanca O (2016) Static and seismic bearing capacity of shallow strip footings. *Soil Dynamics and Earthquake Engineering* 84:204-223, DOI: 10.1016/j.soildyn.2016.02.010

Chen BH, Luo WJ, Xu XY, Hu RQ, Yang XL (2022) Seismic bearing capacity of strip footing with nonlinear mohr-coulomb failure criterion. *International Journal of Geomechanics* 22(10):06022029, DOI: 10.1061/(ASCE)GM.1943-5622.0002521

Coley DA (1999) An introduction to genetic algorithms for scientists and engineers. World Scientific Publishing Company, Singapore, 25-32

Conti R (2018) Simplified formulas for the seismic bearing capacity of shallow strip foundations. *Soil Dynamics and Earthquake Engineering* 104:64-74, DOI: 10.1016/j.soildyn.2017.09.027

Dormieux L, Pecker A (1995) Seismic bearing capacity of foundation on cohesionless soil. *Journal of Geotechnical Engineering* 121(3): 300-303, DOI: 10.1061/(ASCE)0733-9410(1995)121:3(300)

Drescher A, Christopoulos C (1988) Limit analysis slope stability with nonlinear yield condition. *International Journal for Numerical and Analytical Methods in Geomechanics* 12(3):341-345, DOI: 10.1002/nag.1610120307

Fraldi M, Guarracino F (2009) Limit analysis of collapse mechanisms in cavities and tunnels according to the Hoek-Brown failure criterion. *International Journal of Rock Mechanics and Mining Sciences* 46(4):665-673, DOI: 10.1016/j.ijrmms.2008.09.014

Ganesh R, Kumar J (2021) Ultimate bearing capacity of strip and circular foundations using power type yield criterion using the method of stress characteristics. *Computers and Geotechnics* 133:104066, DOI: 10.1016/j.compgeo.2021.104066

Ganesh R, Kumar J (2022). Seismic bearing capacity of strip foundations with nonlinear power-law yield criterion using the stress characteristics method. *Journal of Geotechnical and Geoenvironmental Engineering* 148(11):04022083, DOI: 10.1061/(ASCE)GT.1943-5606.0002867

Gazetas G, Psarropoulos PN, Anastasopoulos I, Gerolymos N (2004) Seismic behaviour of flexible retaining systems subjected to short-duration moderately strong excitation. *Soil Dynamics and Earthquake Engineering* 24(7):537-550, DOI: 10.1016/j.soildyn.2004.02.005

Ghosh P (2008) Upper bound solutions of bearing capacity of strip footing by pseudo-dynamic approach. *Acta Geotech* 3:115-123, DOI: 10.1007/s11440-008-0058-z

Hoek E (1990) Estimating Mohr-Coulomb friction and cohesion values from the Hoek-Brown failure criterion. *In International Journal of Rock Mechanics and Mining Sciences & Geomechanics Abstracts* 27(3):227-229, DOI: 10.1016/0148-9062(90)94333-O

Huang CC (2005) Seismic displacements of soil retaining walls situated on slope. *Journal of Geotechnical and Geoenvironmental Engineering* 131(9):1108-1117, DOI: 10.1061/(ASCE)1090-0241(2005)131:9(1108)

Huang D, Liu J (2016) Upper-bound limit analysis on seismic rotational stability of retaining wall. *KSCE Journal of Civil Engineering* 20(7): 2664-2669, DOI: 10.1007/s12205-016-0471-z

Kobayashi T, Ochiai H, Suyama Y, Aoki S, Yasufuku N, Omine K (2009) Bearing capacity of shallow foundations in a low gravity

environment. *Soils and Foundations* 49(1):115-134, DOI: 10.3208/sandf.49.115

Kumar J, Mohan Rao VBK (2002) Seismic bearing capacity factors for spread foundations. *Geotechnique* 52(2):79-88, DOI: 10.1680/geot.2002.52.2.79

Li YX, Hu YN, Huang F, Li SQ, Sun ZB (2021) A novel method for the stability assessment of soil slopes with multi-layers based on the upper bound limit analysis. *KSCE Journal of Civil Engineering* 25:2855-2864, DOI: 10.1007/s12205-021-1170-y

Liu J, Xu S, Yang XL (2022) Modified pseudo-dynamic bearing capacity of strip footing on rock masses. *Computers and Geotechnics* 150:104897, DOI: 10.1016/j.compgeo.2022.104897

Michalowski RL, Park D (2020) Stability assessment of slopes in rock governed by the Hoek-Brown strength criterion. *International Journal of Rock Mechanics and Mining Sciences* 127:104217, DOI: 10.1016/j.ijrmms.2020.104217

Nadgouda K, Choudhury D (2021) Seismic bearing capacity factor $N_{\gamma e}$ for dry sand beneath strip footing using modified pseudo-dynamic method with composite failure surface. *International Journal of Geotechnical Engineering* 15:171-180, DOI: 10.1080/19386362.2019.1707994

Pane V, Vecchietti A, Cecconi M (2016) A numerical study on the seismic bearing capacity of shallow foundations. *Bulletin of Earthquake Engineering* 14(11):2931-2958, DOI: 10.1007/s10518-016-9937-0

Serrano A, Olalla C, Jimenez R (2016) Analytical bearing capacity of strip footings in weightless materials with power-law failure criteria. *International Journal of Geomechanics* 16(1):04015010, DOI: 10.1061/(ASCE)GM.1943-5622.0000465

Soubra AH (1999) Upper-bound solutions for bearing capacity of foundations. *Journal of Geotechnical and Geoenvironmental Engineering* 125(1):59-68, DOI: 10.1061/(ASCE)1090-0241(1999)125:1(59)

Soufi GR, Chenari RJ, Javankhoshdel S (2021) Conventional vs. modified pseudo-dynamic seismic analyses in the shallow strip footing bearing capacity problem. *Earthquake Engineering and Engineering Vib*ration 20:993-1006, DOI: 10.1007/s11803-021-2064-1

Tavakoli MA, Fathipour H, Payan M, Chenari RJ, Ahmadi H (2022) Modified pseudo-dynamic bearing capacity of shallow foundations subjected to inclined-eccentric combined loading (preprint). *In Review*, DOI: 10.21203/rs.3.rs-1281541/v1

Terzaghi K (1943) Theoretical Soil Mechanics. New York: Wiley

Xu S, Zhou D (2023) Seismic bearing capacity solution for strip footings in unsaturated soils with modified pseudo-dynamic approach. *Mathematics* 11:2692, DOI: 10.3390/math11122692

Yang XL, Huang F (2011) Collapse mechanism of shallow tunnel based on nonlinear Hoek-Brown failure criterion. *Tunnelling and Underground Space Technology* 26(6):686-691, DOI: 10.1016/j.tust.2011.05.008

Yang XL, Li L, Yin JH (2004). Seismic and static stability analysis for rock slopes by a kinematical approach. *Geotechnique* 54(8):543-549, DOI: 10.1680/geot.2004.54.8.543

Yang XL, Wang JM (2011) Ground movement prediction for tunnels using simplified procedure. *Tunnelling and Underground Space Technology* 26(3):462-471, DOI: 10.1016/j.tust.2011.01.002

Yang XL, Yin JH (2004) Slope stability analysis with nonlinear failure criterion. *Journal of Engineering Mechanics* 130(3):267-273, DOI: 10.1061/(ASCE)0733-9399(2004)130:3(267)

Yang XL, Yin JH (2005) Upper bound solution for ultimate bearing capacity with a modified Hoek-Brown failure criterion. *International Journal of Rock Mechanics and Mining Sciences* 42(4):550-560, DOI: 10.1016/j.ijrmms.2005.03.002

Yu L, Lyu C, Wang M, Xu T (2019) Three-dimensional upper bound limit analysis of a deep soil-tunnel subjected to pore pressure based on the nonlinear Mohr-Coulomb criterion. *Computers and Geotechnics* 112:293-301, DOI: 10.1016/j.compgeo.2019.04.025

Zeng X, Steedma RS (1998) Bearing capacity failure of shallow foundations in earthquakes. *Géotechnique* 48(2):235-256, DOI: 10.1680/geot.1998.48.2.235

Zhang XJ, Chen WF (1987) Stability analysis of slopes with general nonlinear failure criterion. *International Journal for Numerical and Analytical Methods in Geomechanics* 11(1):33-50, DOI: 10.1002/nag.1610110104

Zhang DB, Sun WC, Wang CY, Yu BA (2021) Reliability analysis of seismic stability of shield tunnel face under multiple correlated failure modes. *KSCE Journal of Civil Engineering* 18:103562, DOI: 10.1007/s12205-021-2174-3

Zhong JH, Li YX, Yang XL (2022) Estimation of the seismic bearing capacity of shallow strip footings based on a pseudodynamic approach. *International Journal of Geomechanics* 22(9):04022143, DOI: 0.1061/(ASCE)GM.1943-5622.0002459

Zhong JH, Liao H (2022) Stability analysis of 3D deep tunnel face under steady seepage flow condition. *KSCE Journal of Civil Engineering* 26(5):2509-2518, DOI: 10.1007/s12205-022-1907-2

Appendix A

Bilateral symmetry failure mechanism:

$$N_\gamma = -\frac{4}{b^2}\cdot\left[\frac{1}{8}b^2\tan\beta + \frac{\cos(\beta-\varphi_1)}{r_0\cos\varphi_1}\cdot G_1 - \frac{1}{2}\frac{r_n^3\cos\varphi_n\sin(\beta+\theta_a)\cos(\beta+\theta_a)\cos(\beta-\varphi_1)}{r_0\cos\varphi_1\cos(\beta+\theta_a-\varphi_n)}\right] \tag{52}$$

$$N_q = \frac{2}{b}\left[\frac{r_n^2\cos\varphi_n\cos(\beta+\theta_a)\cos(\beta-\varphi_1)}{r_0\cos\varphi_1\cos(\beta+\theta_a-\varphi_n)}\right] \tag{53}$$

$$N_c^{'} = \frac{2}{b}\cdot\left[\frac{b}{2}(\tau_1-\sigma_{n1}\tan\varphi_1)\tan\beta + \frac{\cos(\beta-\varphi_1)}{r_0\cos\varphi_1}\cdot G_2 + (\tau_n-\sigma_{nn}\tan\varphi_n)\frac{r_n^2\cos\varphi_n\sin(\beta+\theta_a)\cos(\beta-\varphi_1)}{r_0\cos\varphi_1\cos(\pi-\beta-\theta_a+\varphi_n)}\right] \tag{54}$$

$$G_1 = \sum_{j=1}^{n} \int_{\theta_{j-1}}^{\theta_j} \int_{o}^{r} \rho^2 \cos(\beta+\theta)\, d\rho\, d\theta$$

$$= \frac{1}{3} \cdot \left(\frac{b}{2\cos\beta}\right)^3 \cdot \frac{\sin(\beta+\sum_{i=1}^{j}\eta_i)e^{3\eta_i \tan\varphi_j} - \sin(\beta+\sum_{i=1}^{j-1}\eta_i) + 3\tan\varphi_j \left[\cos(\beta+\sum_{i=1}^{j}\eta_i)e^{3\eta_i \tan\varphi_j} - \cos(\beta+\sum_{i=1}^{j-1}\eta_i)\right]}{9\tan^2\varphi_j + 1} \tag{56}$$

$$G_2 = \sum_{j=1}^{n} \int_{\theta_{j-1}}^{\theta_j} \left(\tau_j - \sigma_{nj}\tan\varphi_j\right) r^2\, d\theta$$

$$= \sum_{j=1}^{n} (\tau_j - \sigma_{nj}\tan\varphi_j) \cdot \frac{b^2}{4\cos^2\beta} e^{2\sum_{k=1}^{j-1}\eta_k \tan\varphi_k} \cdot \frac{1}{2\tan\varphi_j}(e^{2\eta_j \tan\varphi_j} - 1) \tag{57}$$

Binding conditions:

$$\begin{aligned}
&0 < \beta < \frac{\pi}{2}\\
&0 < \theta_a < \pi\\
&0 < \varphi_i < \frac{\pi}{2}\\
&0 < \eta_i < \frac{\pi}{2}\\
&0 < \beta + \theta_a < \pi\\
&\varphi_n - \beta - \theta_a < -\frac{\pi}{2}\\
&\beta - \frac{\varphi_1}{2} = \frac{\pi}{4}\\
&\eta_1 + \eta_2 + \cdots + \eta_n - \theta_a = 0
\end{aligned} \tag{58}$$

Appendix B

Unilateral failure mechanism (considering seismic forces):

$$\alpha = \arctan\left(k_h(0,t)\right) \tag{57}$$

$$f_1 = \tau_1 - \sigma_{n1}\tan\varphi_1 \tag{58}$$

$$f_2 = \left(\tau_n - \sigma_{nn}\tan\varphi_n\right)\left(\frac{\sin\left(\beta+\theta_a\right)\cos\varphi_n}{\cos\left(\pi-\beta-\theta_a+\varphi_n\right)}\right) \tag{59}$$

$$f_3 = \frac{\cos\left(\beta-\alpha\right)}{\cos\alpha} \tag{60}$$

$$f_4 = \left(\frac{\cos\varphi_n}{\cos\left(\pi-\beta-\theta_a+\varphi_n\right)}\right)\left[k_h(0,t)\sin\left(\pi-\beta-\theta_a\right) - \cos\left(\pi-\beta-\theta_a\right)\right] \tag{61}$$

$$f_5 = \left(\frac{r_0 b^2 \sin\beta\cos\beta\cos\left(\varphi_1-\beta\right)}{2\cos\varphi_1}\right) + J - \left(\frac{r_n^3\cos\varphi_n\sin(\beta+\theta_a)\cos(\pi-\beta-\theta_a)}{2\cos\left(\pi-\beta-\theta_a+\varphi_n\right)}\right) \tag{62}$$

$$f_6 = \frac{1}{\left(C_s^2+S_s^2\right)}\left[\left(C_sI_1+S_sI_2\right)\cos(\omega t) + \left(S_sI_1-C_sI_2\right)\sin(\omega t)\right] \tag{63}$$

$$f_7 = \frac{1}{\left(C_s^2+S_s^2\right)}\left[\left(C_sI_3+S_sI_4\right)\cos(\omega t) + \left(S_sI_3-C_sI_4\right)\sin(\omega t)\right] \tag{64}$$

$$f_8 = \sin\left(\beta+\sum_{k=1}^{i}\eta_k\right)\left[\cot\left(\beta+\sum_{k=1}^{i}\eta_k\right) - \cot\left(\beta+\sum_{k=1}^{i+1}\eta_k\right)\right]e^{\sum_{k=1}^{i}\eta_k\tan\varphi_k} \tag{65}$$

$$f_9=\frac{1}{\left(C_s^2+S_s^2\right)}\left[\left(C_sI_5+S_sI_6\right)\cos(\omega t)+\left(S_sI_5-C_sI_6\right)\sin(\omega t)\right] \tag{66}$$

$$I_1=\int_0^{z_c}\frac{1}{b}\left[1-\frac{\cos\varphi_1}{\sin\beta\cos\left(\beta-\varphi_1\right)}\frac{z}{b}\right]C_{sz}\mathrm{d}z \tag{67}$$

$$I_2=\int_0^{z_c}\frac{1}{b}\left[1-\frac{\cos\varphi_1}{\sin\beta\cos\left(\beta-\varphi_1\right)}\frac{z}{b}\right]S_{sz}\mathrm{d}z \tag{68}$$

$$I_3=\int_0^{z_D}\frac{1}{b}\left[-\frac{\cos\left(\beta-\varphi_1\right)\cos\varphi_n}{\cos\varphi_1\cos\left(\beta+\theta_a-\varphi_n\right)}e^{\sum_{i=1}^{n}\eta_i\tan\varphi_i}+\frac{\cos\varphi_n}{\sin\left(\beta+\theta_a\right)\cos\left(\beta+\theta_a-\varphi_n\right)}\frac{z}{b}\right]C_{sz}\mathrm{d}z \tag{69}$$

$$I_4=\int_0^{z_D}\frac{1}{b}\left[-\frac{\cos\left(\beta-\varphi_1\right)\cos\varphi_n}{\cos\varphi_1\cos\left(\beta+\theta_a-\varphi_n\right)}e^{\sum_{i=1}^{n}\eta_i\tan\varphi_i}+\frac{\cos\varphi_n}{\sin\left(\beta+\theta_a\right)\cos\left(\beta+\theta_a-\varphi_n\right)}\frac{z}{b}\right]S_{sz}\mathrm{d}z \tag{70}$$

$$I_5=\int_0^{z_1}\frac{z}{b^2}C_{sz}\mathrm{d}z \tag{71}$$

$$I_6=\int_0^{z_1}\frac{z}{b^2}S_{sz}\mathrm{d}z \tag{72}$$

$$z_c=\frac{b\cos\left(\beta-\varphi_1\right)}{\cos\varphi_1}\sin\beta \tag{73}$$

$$z_D=\frac{b\cos\left(\beta-\varphi_1\right)\sin\left(\beta+\theta_a\right)}{\cos\varphi_1}e^{\sum_{i=1}^{n}\eta_i\tan\varphi_i} \tag{74}$$

$$z_1=\frac{b\cos\left(\beta-\varphi_1\right)}{\cos\varphi_1}\sin\left(\beta+\sum_{k=1}^{i}\eta_k\right)e^{\sum_{k=1}^{i}\eta_k\tan\varphi_k} \tag{75}$$

$$z_2=\frac{b\cos\left(\beta-\varphi_1\right)}{\cos\varphi_1}\sin\left(\beta+\sum_{k=1}^{i+1}\eta_k\right)e^{\sum_{k=1}^{i+1}\eta_k\tan\varphi_k} \tag{76}$$

$$\begin{aligned}J&=\sum_{j=1}^{n}\int_{\theta_{j-1}}^{\theta_j}\int_0^{r}\rho^2\cos(\beta+\theta)\,d\rho\,d\theta\\&=\frac{1}{3}\cdot(b_e\frac{\cos(\varphi_1-\beta)}{\cos\varphi_1})^3\cdot\frac{\sin(\beta+\sum_{i=1}^{j}\eta_i)e^{3\eta_i\tan\varphi_j}-\sin(\beta+\sum_{i=1}^{j-1}\eta_i)+3\tan\varphi_j\left[\cos(\beta+\sum_{i=1}^{j}\eta_i)e^{3\eta_i\tan\varphi_j}-\cos(\beta+\sum_{i=1}^{j-1}\eta_i)\right]}{9\tan^2\varphi_j+1}\end{aligned} \tag{77}$$

$$\sum_{j=1}^{n}\int_{\theta_{j-1}}^{\theta_j}\left(\tau_j-\sigma_{nj}\tan\varphi_j\right)r^2\,d\theta=\sum_{j=1}^{n}(\tau_j-\sigma_{nj}\tan\varphi_j)\cdot(b_e\frac{\cos(\varphi_1-\beta)}{\cos\varphi_1})^2e^{2\sum_{k=1}^{j-1}\eta_k\tan\varphi_k}\cdot\frac{1}{2\tan\varphi_j}(e^{2\eta_j\tan\varphi_j}-1) \tag{78}$$

Binding conditions:

$$0<\beta<\frac{\pi}{2}$$

$$0<\theta_a<\pi$$

$$0<\varphi_i<\frac{\pi}{2}$$

$$0<\eta_i<\frac{\pi}{2}$$

$$0<\beta-\varphi_1<\frac{\pi}{2}$$

$$\varphi_n-\beta-\theta_a<-\frac{\pi}{2}$$

$$\eta_1+\eta_2+\cdots+\eta_n-\theta_a=0$$